Article

Discovery Medicine 2024; 36(182): 632–645
https://doi.org/10.24976/Discov.Med.202436182.60

Investigating the Spatial Distribution of Proliferating Cells in Primary Ovarian Cancers

Mohamed A.A.A Hegazi[1], Fabio Pasqualini[1,2], Gianluigi Taverna[3], Robert S. Bresalier[4], Maurizio Chiriva-Internati[4,†], Fabio Grizzi[1,2,*,†]

[1]Department of Immunology and Inflammation, IRCCS Humanitas Research Hospital, 20089 Rozzano, Milan, Italy
[2]Department of Biomedical Sciences, Humanitas University, 20072 Pieve Emanuele, Milan, Italy
[3]Department of Urology, Humanitas Mater Domini, 21100 Castellanza, Varese, Italy
[4]Departments of Gastroenterology, Hepatology & Nutrition, Division of Internal Medicine, The University of Texas MD Anderson Cancer Center, Houston, TX 77030, USA
*Correspondence: fabio.grizzi@humanitasresearch.it (Fabio Grizzi)
[†]These authors contributed equally.
Published: 20 March 2024

Background: Ovarian cancer (OC) accounts for about 4% of female cancers globally. While Ki67-immunopositive (Ki67$^+$) cell density is commonly used to assess proliferation in OC, the two-dimensional (2D) distribution pattern of these cells is poorly understood. This study explores the 2D distribution pattern of Ki67$^+$ cells in primary OC tissues and models the proliferation process to improve our understanding of this hallmark of cancer.

Methods: A total of 100 tissue cores, included in a tissue microarray (TMA) representing 5 clear cell carcinomas, 62 serous carcinomas, 10 mucinous adenocarcinomas, 3 endometrioid adenocarcinomas, 10 lymph node metastases from OC, and 10 samples of adjacent normal ovary tissue, were stained using a standardized immunohistochemical protocol. The computer-aided image analysis system assessed the 2D distribution pattern of Ki67$^+$ proliferating cells, providing the cell number and density, patterns of randomness, and cell-to-cell closeness. Three computer models were created to simulate behavior and responses, aiming to gain insights into the variations in the proliferation process.

Results: Significant differences in Ki67$^+$ cell density were found between low- and high-grade serous carcinoma/mucinous adenocarcinomas (p = 0.003 and p = 0.01, respectively). The Nearest Neighbor Index of Ki67$^+$ cells differed significantly between high-grade serous carcinomas and endometrioid adenocarcinomas (p = 0.01), indicating distinct 2D Ki67$^+$ distribution patterns. Proxemics analysis revealed significant differences in Ki67$^+$ cell-to-cell closeness between low- and high-grade serous carcinomas (p = 0.002). Computer models showed varied effects on the overall organization of Ki67$^+$ cells and the ability to preserve the original 2D distribution pattern when altering the location and/or density of Ki67$^+$ cells.

Conclusions: Cell proliferation is a hallmark of OCs. This study provides new evidence that investigating the Ki67$^+$ cell density and 2D distribution pattern can assist in understanding the proliferation status of OCs. Moreover, our computer models suggest that changes in Ki67$^+$ cell density and their location are critical for maintaining the 2D distribution pattern.

Keywords: ovarian cancer; proliferation; Ki67; distribution pattern; spatial analysis; topography

Introduction

Ovarian cancer (OC) ranks seventh in female cancer prevalence and eighth in mortality causes among women globally, with a 49% five-year relative survival rate [1]. The epithelial subtype encompasses up to 95% of all OC cases, and approximately 70% of epithelial OCs are characterized by high-grade serous carcinoma (HGSC). Clear cell carcinomas (CCCs) and endometrioid adenocarcinomas (EAs) each account for 10%, while low-grade serous carcinoma (LGSC) makes up less than 5%, and the mucinous adenocarcinomas (MAs) type represents 3% of cases [1–4]. Tumor recurrence and metastasis are the primary factors contributing to unfavorable clinical outcomes and cancer fatalities, despite patients' initial responsiveness to cytoreductive surgery and subsequent platinum-based chemotherapy [5–9]. Consequently, identifying novel features of tumor initiation and progression is crucial for the prevention, detection, and treatment of OC [10,11]. It is known that cancer cells are capable of maintaining continuous proliferation [12]. In healthy tissues, the synthesis and secretion of growth-promoting signals are regulated, ensuring a balance of cell density and the maintenance of natural tissue structure and function. However, cancer cells deregulate these signals, gaining control over their own growth [12,13]. The specific proliferative signals and their sources within tissues remain largely unknown, mainly due to the temporally and spatially regulated transmission of growth

factor signals. Microscopic OC tissue treated with Ki67 antibodies (a protein expressed at varying levels in all cell cycle phases except for resting cells in phase G_0 [14]) exhibits a complex distribution pattern [15]. This complexity can arise from genetic variation [16], non-genetic factors [17], a combination of both or the presence of persistent cancer cells [18]. Non-genetic heterogeneity may be driven by extrinsic factors (i.e., tissue microenvironment) and intrinsic factors (i.e., variation in protein expression) [19]. Although variability in proliferation has been recognized widely and even taken into account for assessment recommendations, such as the mitotic activity index, numerous studies have utilized Ki67 as a marker for cellular proliferation not only in OC [20–24] but also in various tumor types, focusing on quantifying the spatial attributes of Ki67-immunopositive ($Ki67^+$) cells. Techniques such as Voronoi tessellation [25] and distribution analysis [26,27] have been employed for this purpose. Primarily, the Ki67 marker is instrumental in calculating the Ki67 proliferative index, which represents the proportion of $Ki67^+$ cells within a specified tissue area. This index is particularly significant in the evaluation of neuroendocrine and endocrine tumors, as well as in the assessment of breast and lung cancers, among other malignancies [25,28–37], the extent of proliferative intratumor heterogeneity is still poorly investigated and a method to quantify the two-dimensional (2D) distribution pattern of proliferating cells is currently under investigation [38]. Spatial statistics offer quantitative descriptors of natural variables distributed across space and time [39,40]. The quantitative spatial analysis of $Ki67^+$ cells has become increasingly relevant across a spectrum of pathological conditions, in this study, we applied a combined immunohistochemistry and spatial statistic-based approach to assess the Nearest Neighbor Index (NNI) and the cell-to-cell closeness to investigate the 2D distribution pattern of $Ki67^+$ proliferating cells in OC subtypes. Three computer models were created to simulate behavior and responses, aiming to gain insights into the variations in the proliferation process.

Materials and Methods

Tissue Array

5-µm-thick tissue microarray (TMA) section from USBiomax, Rockville, MD, USA (#BC11115c) which included 100 cases/100 cores (core diameter: 1 mm), containing 5 cases of CCCs, 62 serous carcinomas, 10 MAs, 3 EAs, 10 lymph node metastatic carcinomas, 10 adjacent normal ovary tissue, was investigated. Tissue collection is conducted in accordance with ethical standards, ensuring informed consent from donors, adherence to standard medical practices, and the protection of donor privacy (USBiomax). Patient information, including age, sex, organ, and histological subtype of samples, as well as Tumor, Node, Metastasis (TNM) classification, grade, and stage, was supplied by USBiomax (**Supplementary Table 1**).

Immunohistochemistry

The slide was immersed in a heat retrieval solution (DIVA Antigen Decloaker solution, Biocare Medical, Pacheco, CA, USA) for antigen unmasking using a pressure cooker (Decloaking Chamber™, Biocare Medical, Pacheco, CA, USA), cooled and then treated with 3% hydrogen peroxide solution for 10 minutes at room temperature (RT) to quench endogenous peroxidase. After the incubation with Background Sniper (Biocare Medicals) for 20 min at RT the tissues were treated with antibodies raised against human Ki67 (Clone SP6, Biocare Medicals, dilution 1:50) for 1 hour at RT. Tissues were then incubated with the MACH1 (Biocare Medicals) Mouse Probe for 15 min at RT and subsequently HRP-polymer for 15 min at RT (Biocare Medical, Pacheco, CA, USA). After a 3,3′-Diaminobenzidine (DAB) reaction (Biocare Medical, Pacheco, CA, USA), sections were counterstained with a hematoxylin solution.

TMA Digitalization and $Ki67^+$ Cells Measurements

For image analysis, the slide was digitized at 20x objective magnification using a Zeiss Axioscan.Z1 (Zeiss, Milan, Italy). A newly developed software (Cell Cycle Spatial Analyzer, Version 1.0, Histology Core, IRCCS Humanitas Research Hospital, histology@humanitasresearch.it, Rozzano, Milan, Italy) automatically detects $Ki67^+$ cells on the basis of red, green and blue (RGB) color segmentation, and quantifies the number, density of $Ki67^+$ cells ($Ki67^+$ cells/mm^2) and the size of $Ki67^+$ nuclei together with x-y spatial coordinates. The same image intensity level was used throughout the study.

Computer-Aided Spatial Point Analysis

The NNI measures the degree to which $Ki67^+$ cells are clustered, more clustered than random (MCR), randomly distributed, more dispersed than random (MDR), or *uniformly spaced*, measuring the distances between each $Ki67^+$ cell and its closest neighboring $Ki67^+$ cell and compares these distances to the expected values for a randomly distributed population [41,42] was assessed. The analysis is based on the assumption that all locations have an equal probability of receiving a $Ki67^+$ cell and that all $Ki67^+$ cells are placed independently of one another. The null hypothesis is a random Poisson process, giving a modified exponential nearest neighbor distribution with mean µ,

$$\mu = \frac{\sqrt{A/n}}{2}$$

where A is the sampled area and n is the number of $Ki67^+$ cells. The probability that the distribution follows a Poisson process has been determined in conjunction with the dimensionless NNI value.

$$NNI = \frac{\bar{d}}{\mu} = \frac{2\bar{d}}{\sqrt{A/n}}$$

where $\bar{d}$ is the observed mean distance between nearest neighbors, μ the expected mean distance between nearest neighbors, A the sampled area, and n is the number of Ki67$^+$ cells. NNI has a range that extends from 0 (indicating that the Ki67$^+$ cells are completely clustered), through 1 (Ki67$^+$ cells are randomly dispersed) to a maximum of 2.15 (Ki67$^+$ cells are uniformly spaced), if the ratio value is between 0 and 1 the pattern is MCR and if it is between 1 and 2.15 the pattern is MDR.

The majority of mammalian cells possess a singular nucleus, typically ovoid or spherical in shape, with a diameter ranging from 5 to 20 µm [43]. Utilizing proxemics analysis, which considers the variable of cell-to-cell closeness, the Ki67$^+$ cell population was divided into two groups based on their Euclidean distances. The first group includes cells that are close to each other ($\leq$10 µm). These cells are considered in "intimate condition". The second group includes the cells that are far from each other (>10 µm). These cells are considered in "social condition". The distances were calculated with the formula:

$$d = \sqrt{\left[(x_2 - x_1)^2 + (y_2 - y_1)^2\right]}$$

Where d is the distance between cell A (x_1, y_1) and cell B (x_2, y_2).

The spatial point analysis was performed using RStudio (RStudio Team (2022). RStudio: Integrated Development for R. RStudio, PBC, Boston, MA, USA, URL http://www.rstudio.com/) and (Cell Cycle Spatial Analyzer, Version 1.0, Histology Core, IRCCS Humanitas Research Hospital, histology@humanitasresearch.it, Rozzano, Milan, Italy).

Computer Modeling of 2D Cell Proliferation Pattern Changes in OC

Model 1: The model is aimed at investigating the effect on the initial 2D distribution pattern of adding new cells and their location. At any temporal cycle (n = 100) the model adds 7 or 50 Ki67$^+$ randomly located cells to the original configurations made up of 176 (Case A) or 1382 (Case B) Ki67$^+$ cells.

Model 2: The model is aimed at investigating the effect on the initial 2D distribution pattern of a constant number of newly added cells but differently located. At any temporal cycle (n = 100) the model adds a total of 7 or 50 Ki67$^+$ cells in a random position to the original configuration of Case A and B.

Model 3: The model is aimed at investigating the effect on the initial 2D distribution pattern of removing a constant number differently located. At any temporal cycle (n = 100) the model randomly removes a total of 7 or 50 Ki67$^+$ cells to the original configuration of Case A and B.

In the first and second models, the simulation process involves random sampling of the x and y coordinates from the set of original points within the established pattern. This method ensures that if the coordinates of a newly simulated point coincide with those already present, the model will reinitiate the sampling process. The objective is to generate a distinct new point that can be integrated into the original pattern. Conversely, in the third model, the approach to simulation diverges by focusing on the removal of existing points. This is achieved through a random selection process, where an index is chosen randomly from the array of existing coordinates. Subsequently, the corresponding point is eliminated from the array, thereby altering the original pattern. Throughout all simulations, a specific parameter has been consistently established, wherein the number of elements either added or removed is fixed at either 7 or 50 Ki67$^+$ cells. Additionally, the number of simulations conducted for each model is uniformly set to 100. Modifying these parameters, (the number of Ki67$^+$ cells altered and the total simulations) could potentially yield more comprehensive and detailed insights into the patterns and behaviors characteristic of Ki67$^+$ cells.

Statistical Analysis

All of the data were expressed as mean values ± SD (range). Univariate analysis was performed by means of the *t*-Student test for parametric variables. The relative dispersion (RD) as a percentage is given by the formula:

$$RD = \left(\frac{SD}{mean}\right) \times 100$$

The statistical analysis was performed using JASP Version 0.18.1 (Intel, JASP Team, 2023) and BoxPlotR: a web-tool for the generation of box plots (http://shiny.chemgrid.org/boxplotr/).

Results

In this study, we examined primary OC tissues by employing antibodies targeting Ki67. Our methodology involved a dual approach, utilizing a standardized immunohistochemistry technique along with a computer-aided image analysis system. This allowed us to explore cell proliferation in terms of both density and spatial distribution, as illustrated in Fig. 1.

To analyze these patterns, the TMA slide was digitized and processed through RGB color segmentation and quantifying various parameters such as cell number, density (Ki67$^+$ cells/mm^2), and the size of Ki67$^+$ nuclei, along with their spatial coordinates. Furthermore, using prox-

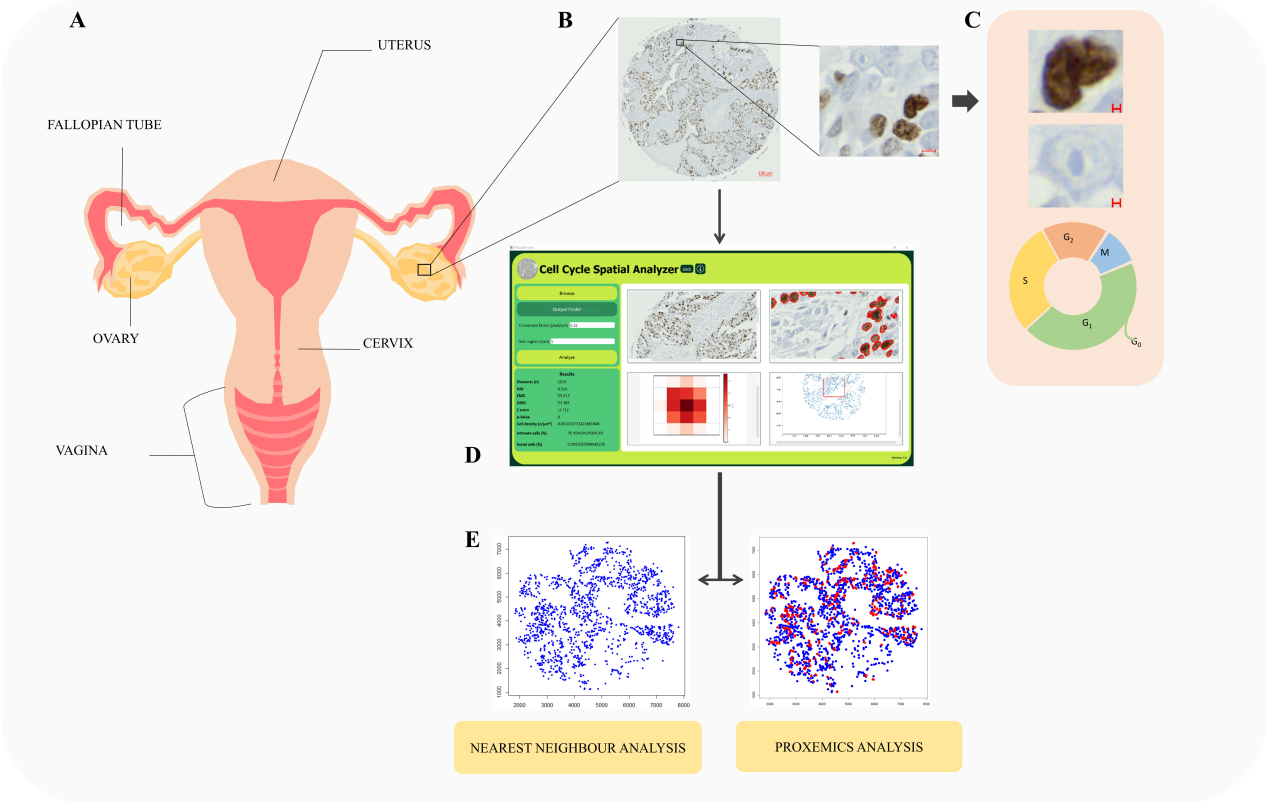

Fig. 1. Two-dimensional analysis of Ki67-immunopositive (Ki67$^+$) cell proliferation in ovarian cancer (OC). The image was created with Microsoft PowerPoint Version 16.78 ©Microsoft 2023 (Redmond, WA, USA). (A) Epithelial ovarian cancer is the seventh most common cancer among women. (B) The traditional method for assessing cell proliferation, which involves labeling tissues with Ki67 is widely accepted Scale bar, 100 µm, inset Scale bar, 5 µm. (C) Ki67 is a protein expressed at varying levels in all cell cycle phases except for resting cells in phase G_0, Scale bar, 2 µm. (D) Digital pathology presents exciting possibilities for improving and automating various tasks in cancer analysis, such as cell proliferation. Studying the specific patterns generated by Ki67$^+$ proliferating cells could provide valuable insights into understanding the links between cell density, spatial variations, responses to treatment and drug resistance in OC. (E) Nearest Neighbour and proxemics (i.e., how space and distance influence cell communication) analyses offer the potential to elucidate the mechanisms underlying the self-organization of Ki67$^+$ cells and their spatial distributions.

emics analysis, the Ki67$^+$ cell population was categorized into two groups based on their Euclidean distances (Fig. 2).

The TMA study included 78 tissue spots from different types of patients: 3 with CCC (mean age: 46 ± 5 years, range: 40–50 years), 8 with LGSCs (mean age: 43 ± 13 years, range: 25–60 years), 54 with HGSCs) (mean age: 51 ± 9 years, range: 22–69 years), 10 with MA (mean age: 42 ± 8 years, range: 29–54 years), and 3 with EA (mean age: 59 ± 10 years, range: 49–69 years). 2 out of 5 CCC cases were excluded due to tissue damage. Lymph node metastatic carcinoma (n = 10) and natural ovary tissue (n = 10) were not investigated. Significant differences were found in Ki67$^+$ cell density and number between LGSC (176 ± 159 Ki67$^+$ cells/mm^2, 77 ± 81 cells) and HGSC (1305 ± 1029 Ki67$^+$ cells/mm^2, 1045 ± 868 cells, p = 0.003), and LGSC and MA (804 ± 623 Ki67$^+$ cells/mm^2, 496 ± 391 cells, p = 0.013 and p = 0.009, respectively) (Fig. 3A,B). No significant difference was found between other subtypes.

A significant difference in the size of Ki67$^+$ nuclei was observed between LGSCs (n = 615, 26 ± 10 µm^2) and HGSCs (n = 56,451, 38 ± 13 µm^2) groups, p = 0.02, consistent with earlier research [44,45]. No significant differences were identified when comparing other subtypes to each other (Fig. 3C).

The mean NNI of Ki67$^+$ cells in HGSCs (1 ± 0.2) was significantly different from EAs (1.4 ± 0.7) (p = 0.01) (Fig. 3D), but not among other subtypes. NNI and Ki67$^+$ cell number and density are independent (R = 0.0007, p = 0.99 and R = –0.07, p = 0.53, respectively). Although no significant differences among OC histotypes, Ki67$^+$ cells in HGSCs and MAs showed a tendency to be MCR than those in LGSCs (Fig. 3D,E). Significant differences were observed in intimate Ki67$^+$ cell-to-cell closeness in LGSCs (11.7 ± 6.1%) versus HGSCs (26.6 ± 12.7%) (p = 0.002) (Fig. 3F–H). When the Ki67$^+$ cell densities were ordered according to their magnitude and compared with the cell-to-cell closeness an irregular line is evident, suggesting that

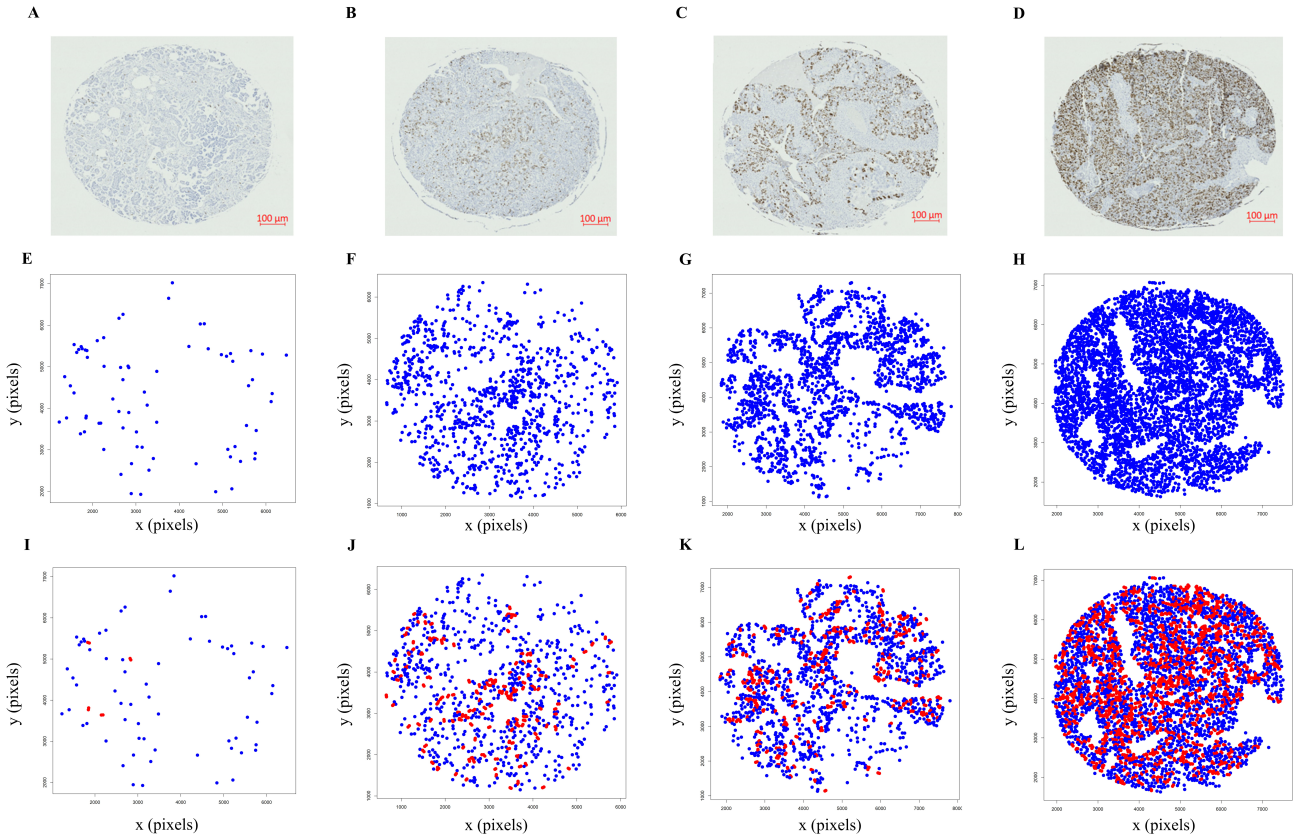

Fig. 2. Microscopic OC tissue treated with Ki67 antibodies exhibits a complex distribution pattern and cell-to-cell closeness features. (A–D) Variability of cell proliferation seen in microscopic OC tissues (from less proliferative A to most proliferative D), Scale bar, 100 µm. (E–H) For each Ki67$^+$ cell, its x-y coordinates have been automatically determined, thus generating an x-y scatter plot. (I–L) The cell-to-cell closeness based on the Euclidean distances categorizes Ki67$^+$ cells in intimate condition (red dots) and in social condition (blue dots).

low or high Ki67$^+$ cell densities can have the same amount of Ki67$^+$ cells in intimate or social conditions (Fig. 3I).

Computer Modeling of 2D Cell Proliferation Pattern Changes in OC

Model 1

In Case A (initial configuration = 176 Ki67$^+$ cells), the 2D Ki67$^+$ cells distribution achieved a random degree on the 32nd cycle with 7 new Ki67$^+$ cells /cycle, or on the 5th with 50 new Ki67$^+$ cells/cycle (Fig. 4A,B). An irregular oscillation between MCR and MDR pattern was observed (Fig. 4C). The mean NNI for adding 7 or 50 cells/cycle was 0.97 $\pm$ 0.05 (range: 0.8–1.05, RD = 5%) and 1 $\pm$ 0.02 (range: 0.83–1.04, RD = 2.4%) respectively ($p <$ 0.001) (Fig. 4D). In Case B (initial configuration made up of 1382 Ki67$^+$ cells), randomness was never achieved with 7 cells/cycle with mean NNI of 0.94 $\pm$ 0.0009 (range: 0.88–0.99, RD = 0.1%) but occurred on the 16th cycle with 50 cells/cycle (Fig. 4E–G) with mean NNI of 1 $\pm$ 0.03 (range: 0.89–1.04, RD = 3%) ($p <$ 0.001) (Fig. 4H).

Analyzing cell-to-cell closeness, for Case A (initial intimate condition = 15.34%), adding 7 or 50 cells/cycle resulted in 15.7 $\pm$ 2.9% (range: 11.02–24.2%, RD = 18%) and 44.6 $\pm$ 18.2% (range: 10.1–70.8%, RD = 41%) cells in intimate conditions respectively ($p <$ 0.001). For Case B (initial intimate condition = 37.6%), these mean values were 39.4 $\pm$ 1.6% (range: 37–43.8%, RD = 4%) and 56.6 $\pm$ 11.5% (range: 37.2–75.3%, RD = 20%) respectively ($p <$ 0.001).

These findings indicate that when a specific number of cells is added to an initial 2D distribution pattern that already contains a high quantity of Ki67$^+$ cells, the arrangement does not achieve a state of randomness. Instead, it retains an organized pattern that is not stochastic in nature. In contrast, when the initial pattern comprises a smaller number of cells, the addition of more cells tends to quickly destabilize this arrangement, eventually leading to a random configuration. Moreover, the percentage of cells in close proximity (intimate condition) tends to remain more consistent where the initial 2D distribution has a higher cell count. This consistency is also reflected by the RD value, particularly when compared to initial patterns with fewer cells.

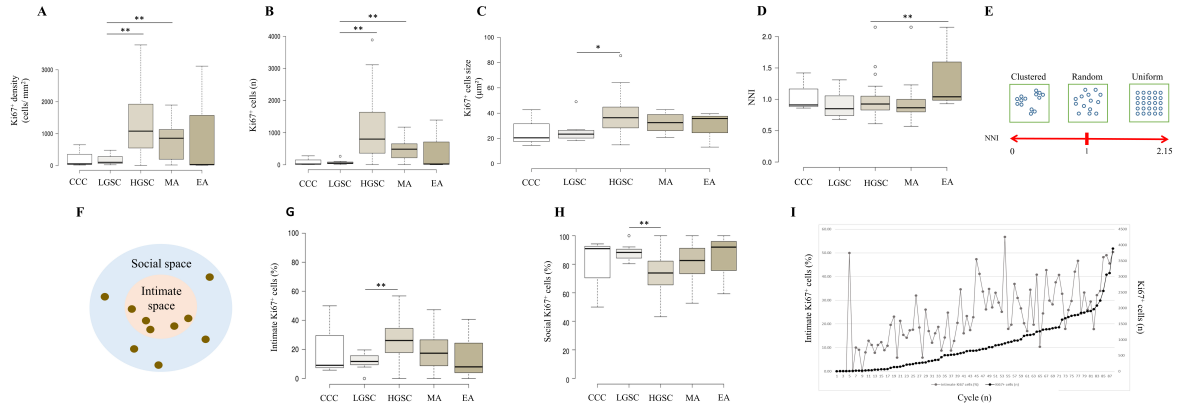

Fig. 3. Comparative analysis of Ki67$^+$ cell features in OC histotypes. (A) Ki67$^+$ cells density evaluation shows a statistically significant difference in low-grade serous carcinomas (LGSCs) versus high-grade serous carcinomas (HGSCs), and LGSCs versus mucinous adenocarcinomas (MAs), no statistical significance was found in clear cell carcinomas (CCCs) and endometrioid adenocarcinomas (EAs). (B) Ki67$^+$ cell number evaluation shows a statistically significant difference in LGSCs versus HGSCs and LGSCs versus MAs. (C) Ki67$^+$ cell size evaluation shows a statistically significant difference in LGSCs versus HGSCs. (D) The Nearest Neighbor Index (NNI) has been found statistically different in HGSCs versus MAs. (E) Three main types of spatial patterns are known. Clustered cells are characterized by a Nearest Neighbor Index (NNI) = 0, randomly dispersed cells by an NNI = 1, or those uniformly spaced by an NNI = 2.15. (F) Schema showing the two zones ("social" space in blue and "intimate" space in red) considered in the proxemics analysis which applies the cell-to-cell closeness variable based on the cell-to-cell Euclidean distance. (G) Proxemic analysis revealed a statistically significant difference in Ki67$^+$ cell percent in intimate conditions in LGSCs versus HGSCs. (H) Proxemic analysis reveals a statistically significant difference in Ki67$^+$ cell percent in social conditions in LGSCs versus HGSCs. (I) When the Ki67$^+$ cell number (black line) was ordered as a crescent series the cell-to-cell closeness (grey line) assumed an irregular behavior, demonstrating their independence. *$p < 0.05$, **$p < 0.01$.

Model 2

100 2D distribution patterns by adding 7 or 50 new cells randomly located in Case A and Case B were generated. In Case A, 7 cells changed the original NNI = 0.83 in 85 out of 100 (85%) of patterns (NNI = 0.85 ± 0.017, range: 0.79–0.88), while 50 cells changed 98 out of 100 (98%) of patterns (NNI = 0.91 ± 0.03, range: 0.83–0.98), $p = 0.0004$ (Fig. 5A). In Case B, the addition of 7 cells changed the original NNI = 0.89 in 57 out of 100 (57%) of patterns, (NNI = 0.89 ± 0.007, range: 0.87–0.9), while the addition of 50 cells modified 65 out of 100 (65%) of patterns (NNI = 0.89 ± 0.01, range: 0.86–0.92, p = NS (Fig. 5A).

These findings suggest that the effect of introducing new Ki67$^+$ cells is greater when the initial Ki67$^+$ cell population is lower. This implies that the starting density, as well as the location of these new cells, significantly influences the 2D distribution pattern.

Model 3

100 2D distribution patterns by removing 7 or 50 Ki67$^+$ cells randomly located in Case A and Case B were generated. In Case A, 7 cells changed the original NNI = 0.83 in 79 out of 100 (79%) of patterns, with mean NNI = 0.8 ± 0.01, range: 0.8–0.9, while the removal of 50 cells changed the original NNI in 91 out of 100 (91%) of patterns, with mean NNI = 0.9 ± 0.04, range: 0.8–1.02, $p = 0.0004$ (Fig. 5B).

In Case B, removing 7 cells changed the original NNI = 0.89 in 4% of patterns, with mean NNI = 0.9 ± 0.002, range: 0.9–0.9, while removing 50 cells changed the original NNI in 17 out of 100 (17%) of patterns, with mean NNI = 0.9 ± 0.004, range: 0.8–0.9, p = NS (Fig. 5B).

These findings suggest that when the initial Ki67$^+$ cell count is lower, the effect of removing Ki67$^+$ cells is significant. This implies that the initial Ki67$^+$ cell density and the location of the new Ki67$^+$ cells greatly affect the 2D distribution pattern. However, compared to Model 2, the act of removal has a lesser effect on changing the 2D distribution pattern.

Discussion

OC is the seventh most frequent cancer in women globally and the eighth highest cause of death among the female population. The forecasts from GLOBOCAN 2020 suggest a significant increase in the worldwide incidence of OC by 2040. It is projected that the incidence rate will rise by about 42%, culminating in approximately 445,721 new cases [46]. Ovarian tumors are characterized by a wide range of histological features and genetic signatures, underscoring the necessity for an elaborate classification framework.

The predominant category, epithelial ovarian tumors, includes multiple subtypes, each identified by unique ge-

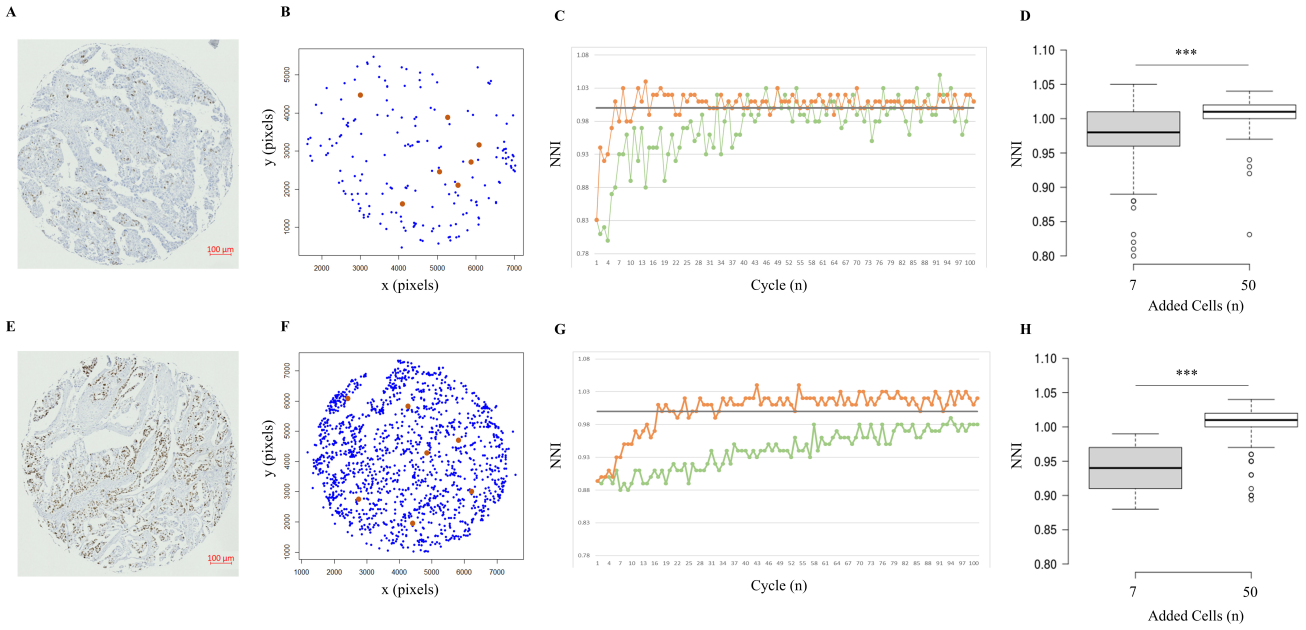

Fig. 4. Computer modeling of cell proliferation by continuously adding new Ki67$^+$ cells. A total of 100 temporal cycles have been considered. At any temporal cycle, the model adds multiple sets of 7 or 50 Ki67$^+$ cells to the original configurations made up of 176 (Case A) or 1382 (Case B) Ki67$^+$ cells. (A,E) Histological images of Case A and Case B, Scale bar, 100 µm. (B,F) For each Ki67$^+$ cell, its x-y spatial coordinates have been automatically determined, thus generating a scatter plot consisting of initial Ki67$^+$ cells (blue dots) and the newly generated Ki67$^+$ cells randomly positioned (orange dots). (C,G) Behavioral plot of the 100 temporal cycles for adding 7 new (green line) or 50 new (orange line) Ki67$^+$ cells, respectively for Case A and Case B, with the Nearest Neighbor Index (NNI) in the y-axis and the "time" points of the simulation in the x-axis. The black line represents the randomness characterized by a NNI = 1. (D,H) A statistically significant difference, respectively in the Case A and Case B, between adding 7 and 50 new Ki67$^+$ cells to the original pattern was found. ***$p < 0.001$.

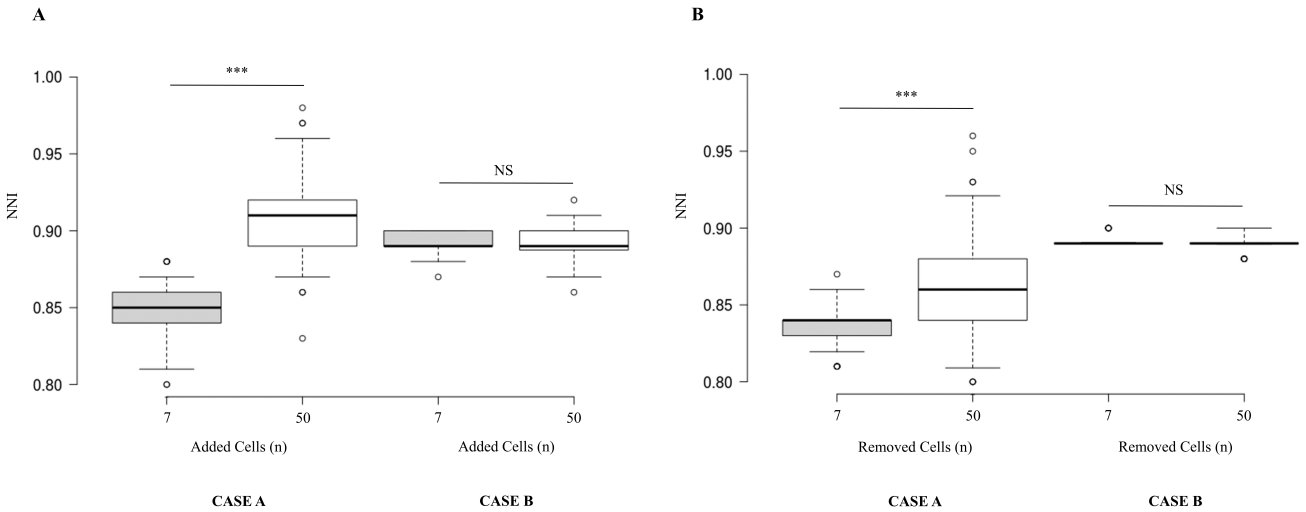

Fig. 5. Computer modeling of cell proliferation by adding and removing new Ki67$^+$ cells. (A) In two simulations by adding 7 or 50 Ki67$^+$ cells for 100 generations (a fixed number for generation) randomly distributed, to the original natural pattern consisting of 176 (Case A) or 1382 (Case B) Ki67$^+$ cells, it has been found a statistically significant difference, respectively in the Case A and Case B, between adding 7 and 50 new Ki67$^+$ cells to the original pattern. (B) In two simulations by removing 7 or 50 Ki67$^+$ cells for 100 generations (a fixed number for generation) randomly distributed, to the original natural Case A or Case B, it has been found a statistically significant difference, respectively in the Case A and Case B, between removing 7 and 50 new Ki67$^+$ cells to the original pattern. NNI, Nearest Neighbor Index, NS, Not significant, ***$p < 0.001$.

netic markers. Within the scope of OC, there exists a varied assortment of histotypes. These are primarily divided into five main groups: HGSCs, LGSCs, EAs, CCCs, and MAs. The most common histotype, HGSC, accounts for about 70% of all OCs. Serous tumors, encompassing serous cystadenoma, adenofibroma, and surface papilloma, frequently exhibit mutations in the breast cancer 1 (*BRCA1*) and *BRCA2* genes. Both LGSCs and HGSCs are associated with a more aggressive form of the disease and may present mutations in the *BRCA*, V-Raf Murine Sarcoma Viral Oncogene Homolog B (*BRAF*), and Kirsten rat sarcoma virus (*KRAS*) genes. In a similar vein, mucinous tumors, including mucinous cystadenoma and adenofibroma, demonstrate a range of genetic variations. Additionally, EA is often linked to Lynch syndrome and microsatellite instability, highlighting their genetic predispositions. Among the gene mutations commonly associated with epithelial OC, four are predominantly identified: tumor protein p53 (*TP53*), *BRCA1/2*, Phosphatidylinositol-4,5-Bisphosphate 3-Kinase Catalytic Subunit Alpha (*PIK3CA*), and *KRAS* [47].

EA represents a diverse group of diseases, each exhibiting unique biological and clinical characteristics. Regardless of their individual differences, a common feature among these histotypes is the tumor cells' capacity for persistent proliferation and evasion of cell death. This shared trait stems from changes at various levels, leading to the disruption of cell cycle regulation and pathways related to cell proliferation [48]. All tumor types share the capacity for sustained chronic proliferation. Cancer develops from the accumulation of genetic alterations that confer neoplastic cells uncontrolled, autonomous growth and resistance to normal regulatory mechanisms of homeostasis. These abilities arise through various mechanisms, and understanding them is crucial for advancing the development of new molecularly targeted therapies, which hold the potential to revolutionize medical oncology. However, the exact nature and origins of the proliferative signals within tissues remain largely unknown. This is primarily due to the belief that growth factor signals, which control cell numbers in tissues, are transmitted in a temporally and spatially regulated manner between neighboring cells. In OC tissues, when observed microscopically and treated with antibodies against Ki67 (a protein extensively used for decades as a marker of cell proliferation in human tumor cells), social variability in cell proliferation is commonly observed [49].

The cellular proliferation status can serve as a biomarker of a tumor's proliferative potential and its sensitivity to chemotherapy, making it a potential prognostic tool. Ki67 is central to this evaluation. Elevated Ki67 antigen expression is correlated with tumor aggression, vascular invasion, metastasis, reserved prognosis, and poor response to chemotherapy. Despite limited data on Ki67 in OC, its prognostic value in HGSC still remains debated [50]. Some studies have identified higher Ki67 expression as a risk factor for survival, associating highly proliferative tumors with a worse outcome. Conversely, other investigations have suggested that HGSC patients with elevated Ki67 expression tend to have longer progression-free survival (PFS), indicating that highly proliferative tumors respond more favorably to first-line chemotherapy. Consequently, the clinical significance of Ki67 in OC warrants further exploration. In a study by Chen *et al.* [24] on HGSC, findings indicated that a Ki67 positivity cut-off of 40% was prognostically discriminative for PFS and Overall Survival (OS). Notably, low tumoral Ki67 expression (<40%) emerged as a risk factor for platinum resistance. Low Ki67 expression has been associated with chemotherapy resistance and disease recurrence in high-grade tumors. It is known that the Ki67 immunostaining pattern exhibits a focal and heterogeneous nature in a greater number of low-grade tumors, contrasting with a more diffuse pattern observed in higher-grade tumors. It is plausible that similar to other spatial phenomena, the distribution of $Ki67^+$ cells might play a pivotal role in the dynamics of OC. While the quantity of cells in the proliferating phase is widely used as an indicator of cell proliferation, it has been noted that more rapid proliferation is not necessarily indicative of tumor progression in HGSC. Asynchrony in cell cycle distribution over time is reflected in the broadening of size distributions. Although cellular distribution patterns and distances are not extensively studied and remain less understood, these patterns offer essential insights into biological processes within tumor tissues related to various tumor characteristics. Studies have reported that investigating the interaction between malignant cells and tumor-associated immune cells through spatial distribution is crucial for identifying potential factors influencing tumor progression, relapse, or outcomes [51]. In the present study, we explored primary OC tissues utilizing antibodies specific to Ki67. Our methodology employed a dual approach, combining a standardized immunohistochemistry technique with a computer-aided image analysis system. This comprehensive approach allowed us to delve into cell proliferation, considering both density and spatial distribution. Building on previous studies that identified "mixed" (i.e., $Ki67^+$ and $Ki67^-$ cells) and "unmixed" (i.e., $Ki67^+$ cells) cellular distribution patterns in melanoma tumor tissues [52], we observed analogous patterns in relation to malignant cells in OC. While cellular distribution patterns and distances have not been extensively studied these patterns furnish crucial information about biological processes within tumor tissues associated with diverse tumor characteristics. The correlation of cellular distribution patterns with clinicopathologic features can enhance our comprehension of tumor biological behavior. Parra *et al.* [51] discovered that not only densities but also distribution patterns and distances from malignant cells to different cell phenotypes could be associated with outcomes.

Here we examine the spatial arrangement of $Ki67^+$ cells in 2D OC tissues and to ascertain if this arrangement

is structured or governed by random mathematical principles. Utilizing a method that combines immunohistochemistry with spatial statistics, the study not only assessed the abundance of $Ki67^+$ cells in terms of their density and number but also quantified their NNI and the proximity between individual cells. The research revealed varying densities of $Ki67^+$ cells between LGSCs and HGSCs (with a significant *p*-value of 0.003), and between LGSCs and MAs (*p*-values of 0.013 and 0.009 respectively). However, no significant differences were found among other subtypes. When analyzing the general organizational pattern and the interactions among $Ki67^+$ cells, the NNI for these cells in HGSCs displayed a significant deviation from that in EA, but not in comparison to other subtypes. The study determined that the NNI and the abundance of $Ki67^+$ cells, in terms of number and density, are unrelated factors. Although no substantial differences were noted across OC histotypes, HGSCs and MAs tended to exhibit more clustered $Ki67^+$ cells compared to LGSCs. Conversely, there were notable differences in the cell-to-cell closeness interaction of $Ki67^+$ cells between LGSCs and HGSCs, as evidenced by a significant *p*-value of 0.002. While previous reports have indicated that LGSCs exhibit a low proliferation rate, this study uniquely demonstrates that the overall organizational pattern and the proximity between cells differ between these two OC histotypes. This finding underscores the significance of evaluating not only the quantity of $Ki67^+$ proliferating cells but also their 2D distribution pattern. Additionally, a notable difference in the size of $Ki67^+$ nuclei was observed between LGSCs and HGSCs groups, aligning with previous studies [44,45]. However, no significant differences were noted when comparing other subtypes with each other. Simulation proves to be a potent tool for assessing and analyzing new system designs, alterations to existing systems, and proposed adjustments to control systems and operating rules. A model, in this context, serves as a representation of a system or process, with a simulation model incorporating time and the dynamic changes that occur over time. Specifically, a discrete model undergoes state changes only at discrete time points rather than continuously. Models may encapsulate logical, mathematical, and structural aspects of the system or process. Simulation becomes particularly advantageous when: (a) the real system is regularized, meaning it is not chaotic and is under control, allowing for the definition and characterization of system components and their interactions; (b) the real system exhibits a certain level of complexity, interaction, or interdependence among components, or sheer size, making it challenging to comprehend in its entirety. This is especially true when predicting the effects of proposed changes is difficult or impossible. Crucial steps in model development involve formulating a list of specific questions that the model should address and establishing a set of measures for evaluating or comparing different conditions of the simulated phenomenon. Despite models not perfectly replicating the "real world", three models have been developed in this study to enhance our understanding of the proliferation dynamics in OCs. Presently, the predominant methods employed in studying cell proliferation patterns involve immunofluorescence and immunohistochemical staining of tissue sections. Consequently, only static images and snapshots of the spatiotemporal evolution can be captured. Recognizing this limitation, the utilization of computer models becomes fundamental to simulate dynamic processes — essentially an infinite sequence of states that would otherwise be examined solely through a series of non-continuous snapshots. These models illustrate that adding or removing $Ki67^+$ cells can significantly affect the organizational structure and the capacity to preserve the original distribution pattern. Specifically, when randomly positioned $Ki67^+$ cells are added or removed, configurations with lower initial densities of $Ki67^+$ cells exhibit more pronounced changes in their NNI. In contrast, configurations with higher initial densities of $Ki67^+$ cells are less susceptible to alterations by the addition or removal of randomly located $Ki67^+$ cells. The results underscore the critical significance of $Ki67^+$ cell density and their 2D spatial arrangement. According to Model 1, when a uniform number of cells is added to an initial 2D distribution pattern containing a high concentration of $Ki67^+$ cells, the proportion of cells in close proximity (intimate condition) tends to remain more stable compared to a pattern that starts with a fewer number of cells. This study supports the existing understanding that LGSC and HGSC are distinct types of tumors. They differ in their origins, pathogenesis, morphology, molecular characteristics, prognostic factors, and response to treatment, as outlined in previous research [53]. Our research revealed that LGSCs possess a smaller quantity of $Ki67^+$ cells, aligning with their documented slow progression rate, especially when compared to HGSCs. Additionally, LGSCs exhibit a reduced proportion of $Ki67^+$ cells in close proximity (intimate condition). This pattern of slow growth in LGSC is attributed to its extended cell cycle duration, which is associated with a favorable prognosis. Conversely, this prolonged cell cycle also contributes to a decreased sensitivity to chemotherapy, an aspect that is considered indicative of a poorer prognosis [54,55]. Based on our findings we hypothesize that increasing the number of cells in intimate condition might improve the response to therapy of LGSCs. It has been also shown that NNA on a relatively small tissue sample is sufficient to produce an accurate picture of the spatial distribution of the underlying population. An advantage that may accrue from the investigation of spatial distribution in addition to incidence is that both techniques may converge on a common explanation for a phenomenon [56,57].

The study presents a scenario where if incidence research points to greater heterogeneity in certain areas, and spatial studies show clustering in these same areas, it could be inferred that the observed phenomenon tends to form

groups. This illustrates how spatial distribution analysis complements incidence studies by providing a different kind of information. In histopathology, the NNA is valuable for understanding the mechanisms behind pattern formation. The NNI measures how much an observation deviates from a theoretically random distribution. Importantly, the NNI is dimensionless, allowing for direct comparison of patterns across various spatial scales. The spatial point analysis sheds light on the interactions among individuals in a population within their complex environment, offering deeper insights than simple density measurements. NNA could reveal new aspects of the intricate relationships between malignant proliferating and non-proliferating cells, as well as other cell types in the microenvironment. Our findings indicate that the spatial arrangement of Ki67$^+$ proliferating cells in 2D tissue sections does not adhere to random mathematical rules. To establish potential links between the topography of Ki67$^+$ patterns and the clinical and pathological characteristics of specific tumors, extensive studies involving large cohorts of subjects are recommended.

Bulloni *et al.* [57] raise an intriguing question regarding the stochastic distribution of Ki67 in tumors. They suggested that the diverse proliferation rates among cell clones [58] could be leveraged to gain deeper insights into tumor biology. Cell proliferation is a key characteristic of OCs and a strong link between Ki67 levels and both recurrence and prognosis of OC has been established [59]. Furthermore, Grabowski *et al.* [22] have identified a correlation between Ki67 expression and several factors in LGSCs, including response to chemotherapy, the time to recurrence after platinum-based chemotherapy, and surgical outcomes. However, there is currently a lack of research on the combined assessment of Ki67$^+$ cell density and their 2D distribution pattern. It has been observed that LGSCs exhibit a distinct clinical profile and a reduced responsiveness to chemotherapy [22]. We found distinct differences between low- and high-grade serous OCs in terms of Ki67$^+$ cell density and their 2D distribution patterns. While the randomness of Ki67$^+$ cells does not significantly vary between these two OC subtypes, the proximity of cells to each other (cell-to-cell closeness) does show a statistical difference, being more pronounced in HGSCs. Conversely, no statistical disparity was found in the cell-to-cell closeness among other examined subtypes, though the degree of randomness did differ significantly between HGSCs and EAs. Despite these promising preliminary results, our study did not investigate the relationship between Ki67 cell density and distribution patterns and the clinical progression of different OC histotypes. Additionally, given the ongoing debate about the use of Ki67 in oncology, particularly concerns about its variable interobserver reproducibility and discrepancies between biopsy and surgical samples due to the unpredictable distribution of proliferating clones within tumors, further research is needed. Specifically, we aim to explore how well findings from a small tissue fraction (such as a TMA core) correspond with observations from entire histological slides.

The combination of NNA with deep learning [60,61] and machine learning algorithms offers a unique method to analyze the diverse Ki67$^+$ cell patterns in 2D tissues. This technique has the potential to automate the classification of these patterns according to their shared features. The NNI, crucial in this setting, measures how patterns differ from random distributions, thus enabling comparisons across various pattern types. This study sheds light on the vital role of Ki67$^+$ cell density and their 2D spatial arrangement in comprehending OC proliferation. Our findings underscore the significance of these factors in maintaining the structure of the system. Investigating the spatial interactions of Ki67$^+$ cells provides insights into their influence on the tumor microenvironment. For instance, Ki67$^+$ cell clusters may reflect areas of intense proliferation, whereas a more scattered distribution might indicate diffuse growth. Analyzing these distribution patterns, especially in response to the addition or removal of cells, underscores the critical impact of spatial organization on the structure and functioning of biological systems. Leveraging spatial statistics and artificial intelligence could further refine this analysis by automating the identification and classification of Ki67$^+$ cells based on characteristics such as density or specific tissue locations. This knowledge could be instrumental in predicting and influencing system behavior under different conditions, thereby informing future therapeutic approaches targeting specific cell groups. Our study's findings have significant potential clinical applications, particularly for diagnosis, prognosis, and treatment of OC. The distinct proliferation patterns, as evidenced by the spatial distribution of Ki67$^+$ cells, could aid in refining the diagnostic criteria for OC subtypes. Such patterns may serve as biomarkers for identifying aggressive tumors, thus influencing treatment decisions. In terms of prognosis, the density and distribution of Ki67$^+$ cells could be indicative of patient outcomes. For example, a higher density might correlate with poorer prognosis or higher recurrence rates. Therefore, incorporating these patterns into prognostic models could enhance the accuracy of patient outcome predictions. Lastly, understanding these proliferation patterns could inform the development of targeted therapies, where treatment strategies are tailored based on the specific proliferation characteristics of the tumor.

The difference in distribution patterns, particularly between LGSCs and HGSCs, may indicate distinct pathophysiological processes [23,24,62–65]. For instance, densely clustered Ki67$^+$ cells in HGSCs could reflect a higher degree of cellular proliferation and aggressiveness, consistent with the generally more advanced and rapidly progressing nature of these tumors. Conversely, the more dispersed Ki67$^+$ cells in LGSCs may correlate with their slower growth and proliferation, aligning with the gener-

ally indolent nature of these tumors. Furthermore, these distribution patterns could be indicative of differences in tumor microenvironmental factors, such as angiogenesis, immune infiltration, and stromal interactions, which are known to influence tumor behavior and progression. The spatial organization of proliferating cells might also suggest variations in genetic and epigenetic regulation across subtypes, potentially offering insights into the distinct molecular pathways driving tumor growth and resistance to treatment. The findings of this study have several implications for the clinical management of OC. The distinct differences observed in $Ki67^+$ cell density and distribution patterns between different OC histotypes, particularly between LGSCs and HGSCs, could aid in refining diagnostic criteria and prognostic assessments. For instance, the unique proliferation patterns and cell-to-cell proximity observed in these subtypes could be used to develop more accurate diagnostic markers, enhancing early detection and stratification of OC cases. Moreover, understanding the spatial organization and proliferation dynamics of these cells offers potential avenues for targeted therapeutic strategies. The variability in $Ki67^+$ cell clusters and their distribution patterns could inform the development of treatments that are tailored to specific tumor microenvironments. This could lead to more effective and personalized approaches in treating OC, potentially improving response rates to chemotherapy and overall patient outcomes. Furthermore, the integration of spatial statistics and machine learning in analyzing these patterns could pave the way for innovative diagnostic and therapeutic tools, harnessing the power of advanced technology to combat OC more effectively.

In addition to Ki67, other proliferation markers such as PCNA, MCM2, and PHH3 are also critical in understanding the proliferative activity in OC. A comparative analysis with these markers could provide a more comprehensive view of tumor biology. While Ki67 is a widely used marker for assessing cell proliferation, other markers like PCNA [66–69] and MCM2 [70–73] offer different perspectives, such as insights into DNA replication processes and cell cycle progression. Comparing the distribution patterns of these markers with Ki67 could reveal synergistic or divergent trends in proliferation, potentially offering new insights into tumor behavior. While the objective of the present research study did not encompass addressing other proliferative markers, we acknowledge the significance of conducting a comparative analysis with such markers. Recognizing this importance, we have outlined a dedicated study specifically designed to explore the spatial interactions among distinct cancer subpopulations identified by specific proliferation markers. The goal is to gain a deeper understanding of the asynchrony among cells undergoing the duplication process. Furthermore, the investigation of the roles of cyclin-dependent kinases in cell-cycle progression and exploring therapeutic strategies for human OC is an important challenge.

The collaborative efforts of mathematicians, biologists, and clinicians [74–76] are crucial in developing a unified quantitative understanding of cancer complexity. This interdisciplinary approach not only aids in clarifying concepts and interpreting both new and existing data, but it also guides the design of alternative experiments and helps in categorizing knowledge about various cancers based on similarities and shared behaviors.

Conclusions

Cell proliferation is a hallmark of OCs. This study provides new evidence that investigating the $Ki67^+$ cell density and 2D distribution pattern can assist in understanding the proliferation status of OCs. Moreover, our computer models suggest that modifications in $Ki67^+$ cell density and their location are critical for maintaining the 2D distribution pattern.

Availability of Data and Materials

The data supporting the conclusions of this paper are included in the manuscript.

Author Contributions

FG, MAAAH and MCI designed the research study and wrote the manuscript; FG, MAAAH and FP performed the research and analyzed the data; FP drafted the manuscript; GT and RSB helped interpret and analyze data, and edited the manuscript; FG and MCI supervised all experiments and edited the manuscript. All authors read and approved the final manuscript. All authors have participated sufficiently in the work and agreed to be accountable for all aspects of the work.

Ethics Approval and Consent to Participate

Not applicable.

Acknowledgment

The authors are grateful to Teri Fields for her assistance in editing this manuscript.

Funding

This research received no external funding.

Conflict of Interest

The authors declare no conflict of interest.

Supplementary Material

Supplementary material associated with this article can be found, in the online version, at https://doi.org/10.24976/Discov.Med.202436182.60.

References

[1] Lheureux S, Braunstein M, Oza AM. Epithelial ovarian cancer: Evolution of management in the era of precision medicine. CA: a Cancer Journal for Clinicians. 2019; 69: 280–304.

[2] Craig O, Nigam A, Dall GV, Gorringe K. Rare Epithelial Ovarian Cancers: Low Grade Serous and Mucinous Carcinomas. Cold Spring Harbor Perspectives in Medicine. 2023; 13: a038190.

[3] Lheureux S, Gourley C, Vergote I, Oza AM. Epithelial ovarian cancer. Lancet (London, England). 2019; 393: 1240–1253.

[4] Schoutrop E, Moyano-Galceran L, Lheureux S, Mattsson J, Lehti K, Dahlstrand H, *et al*. Molecular, cellular and systemic aspects of epithelial ovarian cancer and its tumor microenvironment. Seminars in Cancer Biology. 2022; 86: 207–223.

[5] Hollis RL. Molecular characteristics and clinical behaviour of epithelial ovarian cancers. Cancer Letters. 2023; 555: 216057.

[6] Goon KC, Sheeder J, Post MD, Alldredge J. The impact of adjuvant antihormonal therapy versus observation on recurrence of borderline ovarian tumors: A retrospective cohort study. Gynecologic Oncology Reports. 2023; 47: 101180.

[7] Yee C, Dickson KA, Muntasir MN, Ma Y, Marsh DJ. Three-Dimensional Modelling of Ovarian Cancer: From Cell Lines to Organoids for Discovery and Personalized Medicine. Frontiers in Bioengineering and Biotechnology. 2022; 10: 836984.

[8] Morand S, Devanaboyina M, Staats H, Stanbery L, Nemunaitis J. Ovarian Cancer Immunotherapy and Personalized Medicine. International Journal of Molecular Sciences. 2021; 22: 6532.

[9] Luo Y, Shreeder B, Jenkins JW, Shi H, Lamichhane P, Zhou K, *et al*. Th17-inducing dendritic cell vaccines stimulate effective CD4 T cell-dependent antitumor immunity in ovarian cancer that overcomes resistance to immune checkpoint blockade. Journal for Immunotherapy of Cancer. 2023; 11: e007661.

[10] Cunnea P, Curry EW, Christie EL, Nixon K, Kwok CH, Pandey A, *et al*. Spatial and temporal intra-tumoral heterogeneity in advanced HGSOC: Implications for surgical and clinical outcomes. Cell Reports. Medicine. 2023; 4: 101055.

[11] Yu P, Wang Y, Yuan D, Sun Y, Qin S, Li T. Vascular normalization: reshaping the tumor microenvironment and augmenting antitumor immunity for ovarian cancer. Frontiers in Immunology. 2023; 14: 1276694.

[12] Hanahan D, Weinberg RA. Hallmarks of cancer: the next generation. Cell. 2011; 144: 646–674.

[13] Floor SL, Dumont JE, Maenhaut C, Raspe E. Hallmarks of cancer: of all cancer cells, all the time? Trends in Molecular Medicine. 2012; 18: 509–515.

[14] Sasaki K, Murakami T, Kawasaki M, Takahashi M. The cell cycle associated change of the Ki-67 reactive nuclear antigen expression. Journal of Cellular Physiology. 1987; 133: 579–584.

[15] Dias EP, Oliveira NSC, Serra-Campos AO, da Silva AKF, da Silva LE, Cunha KS. A novel evaluation method for Ki-67 immunostaining in paraffin-embedded tissues. Virchows Archiv: an International Journal of Pathology. 2021; 479: 121–131.

[16] Marusyk A, Almendro V, Polyak K. Intra-tumour heterogeneity: a looking glass for cancer? Nature Reviews. Cancer. 2012; 12: 323–334.

[17] Huang S. Non-genetic heterogeneity of cells in development: more than just noise. Development (Cambridge, England). 2009; 136: 3853–3862.

[18] Shen S, Vagner S, Robert C. Persistent Cancer Cells: The Deadly Survivors. Cell. 2020; 183: 860–874.

[19] Gough A, Stern AM, Maier J, Lezon T, Shun TY, Chennubhotla C, *et al*. Biologically Relevant Heterogeneity: Metrics and Practical Insights. SLAS Discovery: Advancing Life Sciences R & D. 2017; 22: 213–237.

[20] Wan S, Su C, Wang Y, Ding J, Jiang Q, Ding H, *et al*. Prognostic value of Ki-67 in patients with ovarian cancer. European Journal of Gynaecological Oncology. 2023; 1: 6.

[21] Mahadevappa A, Krishna SM, Vimala MG. Diagnostic and Prognostic Significance of Ki-67 Immunohistochemical Expression in Surface Epithelial Ovarian Carcinoma. Journal of Clinical and Diagnostic Research: JCDR. 2017; 11: EC08–EC12.

[22] Grabowski JP, Martinez Vila C, Richter R, Taube E, Plett H, Braicu E, *et al*. Ki67 expression as a predictor of chemotherapy outcome in low-grade serous ovarian cancer. International Journal of Gynecological Cancer: Official Journal of the International Gynecological Cancer Society. 2020; 30: 498–503.

[23] Rödel F, Zhou S, Győrffy B, Raab M, Sanhaji M, Mandal R, *et al*. The Prognostic Relevance of the Proliferation Markers Ki-67 and Plk1 in Early-Stage Ovarian Cancer Patients With Serous, Low-Grade Carcinoma Based on mRNA and Protein Expression. Frontiers in Oncology. 2020; 10: 558932.

[24] Chen M, Yao S, Cao Q, Xia M, Liu J, He M. The prognostic value of Ki67 in ovarian high-grade serous carcinoma: an 11-year cohort study of Chinese patients. Oncotarget. 2016; 8: 107877–107885.

[25] Khojasteh M, Buys TPH, LeRiche J, Lam S, Guillaud M, MacAulay C. A framework for quantitative assessment of Ki67 distribution in preneoplastic bronchial epithelial lesions. Analytical and Quantitative Cytology and Histology. 2012; 34: 120–138.

[26] Bulloni M, Sandrini G, Stacchiotti I, Barberis M, Calabrese F, Carvalho L, *et al*. Automated Analysis of Proliferating Cells Spatial Organisation Predicts Prognosis in Lung Neuroendocrine Neoplasms. Cancers. 2021; 13: 4875.

[27] Gaglia G, Kabraji S, Rammos D, Dai Y, Verma A, Wang S, *et al*. Temporal and spatial topography of cell proliferation in cancer. Nature Cell Biology. 2022; 24: 316–326.

[28] La Rosa S. Diagnostic, Prognostic, and Predictive Role of Ki67 Proliferative Index in Neuroendocrine and Endocrine Neoplasms: Past, Present, and Future. Endocrine Pathology. 2023; 34: 79–97.

[29] Nielsen TO, Leung SCY, Rimm DL, Dodson A, Acs B, Badve S, *et al*. Assessment of Ki67 in Breast Cancer: Updated Recommendations From the International Ki67 in Breast Cancer Working Group. Journal of the National Cancer Institute. 2021; 113: 808–819.

[30] Liu SZ, Staats PN, Goicochea L, Alexiev BA, Shah N, Dixon R, *et al*. Automated quantification of Ki-67 proliferative index of excised neuroendocrine tumors of the lung. Diagnostic Pathology. 2014; 9: 174.

[31] Davey MG, Hynes SO, Kerin MJ, Miller N, Lowery AJ. Ki-67 as a Prognostic Biomarker in Invasive Breast Cancer. Cancers. 2021; 13: 4455.

[32] Saha M, Chakraborty C, Arun I, Ahmed R, Chatterjee S. An Advanced Deep Learning Approach for Ki-67 Stained Hotspot Detection and Proliferation Rate Scoring for Prognostic Evaluation of Breast Cancer. Scientific Reports. 2017; 7: 3213.

[33] Tao M, Chen S, Zhang X, Zhou Q. Ki-67 labeling index is a predictive marker for a pathological complete response to neoadjuvant chemotherapy in breast cancer: A meta-analysis. Medicine. 2017; 96: e9384.

[34] Tan AS, Yeong JPS, Lai CPT, Ong CHC, Lee B, Lim JCT, *et al*. The role of Ki-67 in Asian triple negative breast cancers: a novel combinatory panel approach. Virchows Archiv: an International Journal of Pathology. 2019; 475: 709–725.

[35] Fulawka L, Blaszczyk J, Tabakov M, Halon A. Assessment of Ki-67 proliferation index with deep learning in DCIS (ductal carcinoma in situ). Scientific Reports. 2022; 12: 3166.

[36] Ishibashi N, Maebayashi T, Aizawa T, Sakaguchi M, Nishimaki H, Masuda S. Correlation between the Ki-67 proliferation index and response to radiation therapy in small cell lung cancer. Ra-

diation Oncology (London, England). 2017; 12: 16.
[37] Mestrum SGC, Cremers EMP, de Wit NCJ, Drent RJM, Ramaekers FCS, Hopman AHN, *et al*. Integration of the Ki-67 proliferation index into the Ogata score improves its diagnostic sensitivity for low-grade myelodysplastic syndromes. Leukemia Research. 2022; 113: 106789.
[38] Chervoneva I, Peck AR, Yi M, Freydin B, Rui H. Quantification of spatial tumor heterogeneity in immunohistochemistry staining images. Bioinformatics (Oxford, England). 2021; 37: 1452–1460.
[39] Hart SP, Usinowicz J, Levine JM. The spatial scales of species coexistence. Nature Ecology & Evolution. 2017; 1: 1066–1073.
[40] Wallet F, Dussert C. Multifactorial comparative study of spatial point pattern analysis methods. Journal of Theoretical Biology. 1997; 187: 437–447.
[41] Jacquez GM. Disease cluster statistics for imprecise space-time locations. Statistics in Medicine. 1996; 15: 873–885.
[42] Clark PJ, Evans FC. Distance to Nearest Neighbor as a Measure of Spatial Relationships in Populations. Ecology. 1954; 35: 445–453.
[43] Lammerding J. Mechanics of the nucleus. Comprehensive Physiology. 2011; 1: 783–807.
[44] Hsu CY, Kurman RJ, Vang R, Wang TL, Baak J, Shih IM. Nuclear size distinguishes low- from high-grade ovarian serous carcinoma and predicts outcome. Human Pathology. 2005; 36: 1049–1054.
[45] Singh I, Lele TP. Nuclear Morphological Abnormalities in Cancer: A Search for Unifying Mechanisms. Results and Problems in Cell Differentiation. 2022; 70: 443–467.
[46] Maioru OV, Radoi VE, Coman MC, Hotinceanu IA, Dan A, Eftenoiu AE, *et al*. Developments in Genetics: Better Management of Ovarian Cancer Patients. International Journal of Molecular Sciences. 2023; 24: 15987.
[47] Radu MR, Prădatu A, Duică F, Micu R, Creţoiu SM, Suciu N, *et al*. Ovarian Cancer: Biomarkers and Targeted Therapy. Biomedicines. 2021; 9: 693.
[48] López-Reig R, López-Guerrero JA. The hallmarks of ovarian cancer: proliferation and cell growth. EJC Supplements. 2020; 15: 27–37.
[49] Sun X, Kaufman PD. Ki-67: more than a proliferation marker. Chromosoma. 2018; 127: 175–186.
[50] Kuhn E, Kurman RJ, Sehdev AS, Shih IM. Ki-67 labeling index as an adjunct in the diagnosis of serous tubal intraepithelial carcinoma. International Journal of Gynecological Pathology: Official Journal of the International Society of Gynecological Pathologists. 2012; 31: 416–422.
[51] Parra ER, Zhang J, Jiang M, Tamegnon A, Pandurengan RK, Behrens C, *et al*. Immune cellular patterns of distribution affect outcomes of patients with non-small cell lung cancer. Nature Communications. 2023; 14: 2364.
[52] Cooper ZA, Reuben A, Spencer CN, Prieto PA, Austin-Breneman JL, Jiang H, *et al*. Distinct clinical patterns and immune infiltrates are observed at time of progression on targeted therapy versus immune checkpoint blockade for melanoma. Oncoimmunology. 2016; 5: e1136044.
[53] Němejcová K, Šafanda A, Bártů MK, Michálková R, Drozenová J, Fabian P, *et al*. A comprehensive immunohistochemical analysis of 26 markers in 250 cases of serous ovarian tumors. Diagnostic Pathology. 2023; 18: 32.
[54] Romero I, Sun CC, Wong KK, Bast RC, Jr, Gershenson DM. Low-grade serous carcinoma: new concepts and emerging therapies. Gynecologic Oncology. 2013; 130: 660–666.
[55] Bodurka DC, Deavers MT, Tian C, Sun CC, Malpica A, Coleman RL, *et al*. Reclassification of serous ovarian carcinoma by a 2-tier system: a Gynecologic Oncology Group Study. Cancer. 2012; 118: 3087–3094.
[56] Maisel BA, Yi M, Peck AR, Sun Y, Hooke JA, Kovatich AJ, *et al*. Spatial Metrics of Interaction between CD163-Positive Macrophages and Cancer Cells and Progression-Free Survival in Chemo-Treated Breast Cancer. Cancers. 2022; 14: 308.
[57] Bulloni M, Pattini L, Pelosi G. Intratumor Distribution of Ki-67 Antigen Beyond Labeling Index for Clinical Decision-Making: A New Way of Counting. JTO Clinical and Research Reports. 2021; 2: 100207.
[58] Pelosi G, Bianchi F, Hofman P, Pattini L, Ströbel P, Calabrese F, *et al*. Recent advances in the molecular landscape of lung neuroendocrine tumors. Expert Review of Molecular Diagnostics. 2019; 19: 281–297.
[59] Qiu D, Cai W, Zhang Z, Li H, Zhou D. High Ki-67 expression is significantly associated with poor prognosis of ovarian cancer patients: evidence from a meta-analysis. Archives of Gynecology and Obstetrics. 2019; 299: 1415–1427.
[60] LeCun Y, Bengio Y, Hinton G. Deep learning. Nature. 2015; 521: 436–444.
[61] Farahani H, Boschman J, Farnell D, Darbandsari A, Zhang A, Ahmadvand P, *et al*. Deep learning-based histotype diagnosis of ovarian carcinoma whole-slide pathology images. Modern Pathology: an Official Journal of the United States and Canadian Academy of Pathology, Inc. 2022; 35: 1983–1990.
[62] Babaier A, Mal H, Alselwi W, Ghatage P. Low-Grade Serous Carcinoma of the Ovary: The Current Status. Diagnostics (Basel, Switzerland). 2022; 12: 458.
[63] Vang R, Shih IM, Kurman RJ. Ovarian low-grade and high-grade serous carcinoma: pathogenesis, clinicopathologic and molecular biologic features, and diagnostic problems. Advances in Anatomic Pathology. 2009; 16: 267–282.
[64] Grisham RN, Slomovitz BM, Andrews N, Banerjee S, Brown J, Carey MS, *et al*. Low-grade serous ovarian cancer: expert consensus report on the state of the science. International Journal of Gynecological Cancer: Official Journal of the International Gynecological Cancer Society. 2023; 33: 1331–1344.
[65] Mehra P, Aditi S, Prasad KM, Bariar NK. Histomorphological Analysis of Ovarian Neoplasms According to the 2020 WHO Classification of Ovarian Tumors: A Distribution Pattern in a Tertiary Care Center. Cureus. 2023; 15: e38273.
[66] Kelman Z. PCNA: structure, functions and interactions. Oncogene. 1997; 14: 629–640.
[67] Paunesku T, Mittal S, Protić M, Oryhon J, Korolev SV, Joachimiak A, *et al*. Proliferating cell nuclear antigen (PCNA): ringmaster of the genome. International Journal of Radiation Biology. 2001; 77: 1007–1021.
[68] González-Magaña A, Blanco FJ. Human PCNA Structure, Function and Interactions. Biomolecules. 2020; 10: 570.
[69] Cardano M, Tribioli C, Prosperi E. Targeting Proliferating Cell Nuclear Antigen (PCNA) as an Effective Strategy to Inhibit Tumor Cell Proliferation. Current Cancer Drug Targets. 2020; 20: 240–252.
[70] Sun Y, Cheng Z, Liu S. MCM2 in human cancer: functions, mechanisms, and clinical significance. Molecular Medicine (Cambridge, Mass.). 2022; 28: 128.
[71] Petryk N, Dalby M, Wenger A, Stromme CB, Strandsby A, Andersson R, *et al*. MCM2 promotes symmetric inheritance of modified histones during DNA replication. Science (New York, N.Y.). 2018; 361: 1389–1392.
[72] Ambinder RF, Newman C, Hayward GS, Biggar R, Melbye M, Kestens L, *et al*. Lack of association of cytomegalovirus with endemic African Kaposi's sarcoma. The Journal of Infectious Diseases. 1987; 156: 193–197.
[73] Kaur G, Balasubramaniam SD, Lee YJ, Balakrishnan V, Oon CE. Minichromosome Maintenance Complex (MCM) Genes Profiling and MCM2 Protein Expression in Cervical Cancer Development. Asian Pacific Journal of Cancer Prevention: APJCP.

2019; 20: 3043–3049.

[74] Grizzi F, Spadaccini M, Chiriva-Internati M, Hegazi MAAA, Bresalier RS, Hassan C, *et al*. Fractal nature of human gastrointestinal system: Exploring a new era. World Journal of Gastroenterology. 2023; 29: 4036–4052.

[75] Orsulic S, John J, Walts AE, Gertych A. Computational pathology in ovarian cancer. Frontiers in Oncology. 2022; 12: 924945.

[76] Malik MZ, Chirom K, Ali S, Ishrat R, Somvanshi P, Singh RKB. Methodology of predicting novel key regulators in ovarian cancer network: a network theoretical approach. BMC Cancer. 2019; 19: 1129.